

THE MORPHOLOGY OF THE RICH SUPERCLUSTER 1451 + 22

ROBIN CIARDULLO¹

Department of Terrestrial Magnetism, Carnegie Institution of Washington

Received 1987 January 2; accepted 1987 April 6

ABSTRACT

The morphological properties of the rich supercluster 1451 + 22 are investigated using photographic galaxy photometry in a two-color system especially sensitive to redshift. By measuring $\sim 125,000$ galaxies in five Palomar Schmidt fields, the supercluster's shape, density profile, density contrast, and galaxy population are found. The data suggest that the structure of 1451 + 22 is that of a face-on pancake, flattened against the plane of the sky, although spherical models are not ruled out. Filaments which are rich in early-type galaxies do exist, but most of the supercluster mass lies outside these regions. In addition, 1451 + 22 may have a core-halo structure, with the central degree containing a much higher galaxy density and a larger percentage of elliptical and S0 galaxies than the outer regions. If 1451 + 22 is flat, the mean luminosity density contrast of the supercluster over the field is $\rho/\rho_{\text{field}} \sim 10$, and the total mass of the system is probably $M > 10^{16} M_{\odot}$. If the supercluster is quasi-spherical, the observed density contrast is $\rho/\rho_{\text{field}} \sim 5$, implying a total mass-to-light for the supercluster of $(M/L)_{\odot} \sim 130$, and a cosmological density parameter $\Omega \sim 0.3$.

Subject headings: cosmology — galaxies: clustering — galaxies: photometry

I. INTRODUCTION

The characterization of supercluster morphology is one of the most important unanswered questions in observational cosmology. Because superclusters are unrelaxed, the distribution of matter within them today reflects the conditions at the epoch of galaxy formation, thereby providing a direct measure of the primordial density perturbations. Furthermore, if these fluctuations can be properly modeled, redshift measurements of supercluster galaxies can lead to the overall supercluster potential and the cosmological density parameter Ω_0 . Thus, superclusters can allow us to probe both the distant past and the future of the universe.

Despite their importance, superclusters are extremely difficult to study because of their size. Magnitude-limited redshift surveys in the Local Supercluster (de Vaucouleurs 1975*a, b*; Tully 1982), Coma/Abell 1367 (Gregory and Thompson 1978; Fontanelli 1984) Hercules/Abell 2197 (Tarenghi *et al.* 1979, 1980; Chincarini, Rood, and Thompson 1981), Perseus (Gregory, Thompson, and Tift 1981), Horologium-Reticulum (Lucey *et al.* 1983), and Bootes (Kirschner *et al.* 1981) have provided intriguing evidence for the existence of large-scale disklike and filamentary structures surrounded by voids. Yet these superclusters are just the nearest systems, not the richest, and the vagaries of Galactic extinction make a complete understanding of the morphologies difficult. When one attempts to study more distant systems, the faint magnitudes involved make redshift surveys much harder, if not impossible to perform. A different method is needed to investigate the richest superclusters, which are at high redshift.

This paper is concerned with probing a rich supercluster's density profile, density contrast, cluster content, and galaxy content through the use of two-filter photographic photometry over a wide field. The supercluster chosen for this study is

1451 + 22, one of the richest superclusters known, and one for which there is substantial dynamical information available (Ciardullo *et al.* 1983, hereafter CFBH). Two different approaches will be used. The supercluster's structure and cluster content will be investigated by studying the distribution of early-type galaxies via the color-redshift relation for ellipticals; its density profile, density contrast, and range of galaxy types will be explored using the color-magnitude diagram and galaxy counts. As a comparison and a control on the analysis, two other regions over 45° away on the sky, but at the same Galactic latitude, will also be analyzed. All supercluster properties will be measured relative to these control fields.

a) Known Properties of the Supercluster

Supercluster 1451 + 22 lies at a redshift of $z \approx 0.115$ and contains five richness class 1 and two richness class 0 Abell clusters (Abell 1958) within a 2.7 radius arranged in roughly an "X" pattern (cf. Fig. 4*a* of CFBH). The richest of these clusters is Abell 1986, which is located at the center of the "X." Abell 2036, another richness 0 cluster at the same redshift as the supercluster, lies 5.8 southeast of the center along one of the axes of the system and may also be associated with the supercluster. Scattered between these rich clusters is a large collection of poor clusters and groups, found through the identification of bright cD and E galaxies. The entire system stretches out over a linear distance greater than $50h^{-1}$ Mpc and, like most superclusters, exhibits a high density contrast in redshift space over its surroundings. The most remarkable feature of the supercluster, however, is its exceedingly small velocity dispersion. The redshifts of 23 groups and clusters within the supercluster imply a line-of-sight velocity dispersion of just $\sim 450 \text{ km s}^{-1}$ (CFBH).

From the velocity data, two conclusions are possible. If the supercluster began as a quasi-spherical density perturbation, the small velocity dispersion must imply local slowing of the Hubble expansion. If this is the case, the matter density in the supercluster can be found by modeling its dynamics, and the measurement of the supercluster density contrast yields Ω_0

¹ Guest Observer, Palomar Observatory; Guest Investigator, Automatic Plate Measuring Facility, Institute for Astronomy, Cambridge, England; Visiting Astronomer, Kitt Peak National Observatory, which is operated by the Association of Universities for Research in Astronomy, Inc., under contract with the National Science Foundation.

TABLE 1
PALOMAR SCHMIDT OBSERVATIONS

Plate	Quadrant	$\alpha(1950)$	$\delta(1950)$	Date 1982	UT	Hour Angle	Filter	Exposure (minutes)
29506.....	Control 1	12 ^h 12 ^m 15 ^s	53°42'45"	Apr 23	0522	-0°36'	J	120
29507.....	Control 1	12 12 15	53 42 45	Apr 23	0705	1 07	F	60
29508.....	Supercluster 3	15 02 13	20 02 07	Apr 23	0902	0 15	J	150
29509.....	Supercluster 3	15 02 13	20 02 07	Apr 23	1058	2 13	F	60
29510.....	Control 2	11 36 42	52 27 53	Apr 24	0410	1 06	F	60
29511.....	Supercluster 1	14 39 32	24 45 05	Apr 24	0608	-2 13	J	150
29512.....	Supercluster 1	14 39 32	24 45 05	Apr 24	0805	-0 15	F	60
29514.....	Supercluster 3	15 02 13	20 02 07	Apr 24	1142	3 00	F	30
29515.....	Control 2	11 36 42	52 27 53	Apr 25	0502	-0 12	J	150
29517.....	Supercluster 4	14 38 52	19 08 58	Apr 25	0857	0 41	J	150
29518.....	Supercluster 4	14 38 52	19 08 58	Apr 25	1053	2 38	F	60

(Ford *et al.* 1981). If, however, the small velocity dispersion is not due to Hubble slowing, but instead reflects the true shape of the supercluster, 1451+22 would then be a thin, face-on pancake, such as might be formed in the dissipative collapse models of Zel'dovich (1978) and Doroshkevich *et al.* (1974, 1980). The best method to test between these two alternatives is through measurements of the supercluster's density profile.

II. OBSERVATIONS AND REDUCTIONS

Three quadrants of 1451+22, along with two control fields positioned 45° away on the sky, were photographed with the Palomar 1.3 m Schmidt telescope in 1982 April. A log of these observations appears in Table 1. The blue photographic color, hereafter called *J*, was formed using a Wratten 32 filter placed in front of a IIIa-J plate. The red color, hereafter designated *F*, was produced by combining a Wratten 22 filter with a IIIa-F plate. These bandpasses, which were chosen to maximize the color-redshift sensitivity for E and S0 galaxies in the supercluster, are shown in Figure 1. All the plates were taken under photometric conditions with 1"-2" seeing.

The initial plate reduction was accomplished with the Automatic Plate Measuring (APM) Facility of Cambridge, England (Kibblewhite 1980). This machine digitizes photographic plates with a high-speed precision microphotometer using an 8 μ m focused laser spot which is positioned with deflecting mirrors.

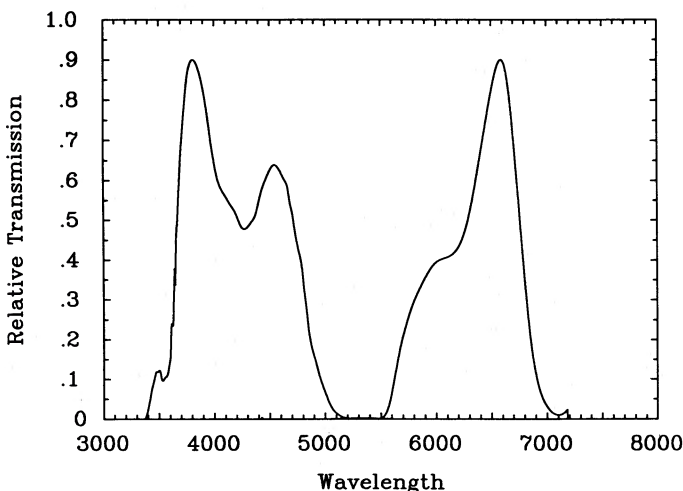


FIG. 1.—Filter response function for the *JF* photographic system. The color-redshift relation for $z \sim 0.1$ is steepened by having the blue (*J*) cutoff at ~ 5000 Å.

In a two-pass process, the APM's special hardware detects all plate images above the background modal sky and describes them through their first and second moments, their peak and total plate densities, and eight areal profiles spaced logarithmically at fixed density levels.

Once the five plate pairs in the survey were measured, a plate comparison program was applied to the data to match the corresponding *J* and *F* images and reject objects not appearing on both plates. The resulting merged catalog for the five Palomar Schmidt fields contained $\sim 250,000$ objects.

The first step in the analysis of this catalog was to separate the galaxies from the stars. This required the use of an image-classifying algorithm. Because of the nature of the merged catalog, two separate procedures were used. At the time of the plate measurements, before any object matching was performed, a statistical clustering algorithm developed by the APM group was run on the raw image data. Each object in the merged catalog thus had two classifications, one for the *J* image and one for the *F* image. For most of the objects the two classifications agreed, and this estimate was adopted. For many of the faintest images, however, disagreement arose. When this happened, a Bayesian scheme which employed 10 discrimination variables and a training set of over 1000 objects decided the classification. The discrimination variables are listed below:

$$\begin{aligned}
 v_1 &= A_{\text{tot}}/I_{\text{tot}} \quad (F \text{ plate}), & v_2 &= A_{\text{tot}}/I_{\text{tot}} \quad (J \text{ plate}), \\
 v_3 &= \sigma_{\text{rr}}/I_{\text{tot}} \quad (F \text{ plate}), & v_4 &= \sigma_{\text{rr}}/I_{\text{tot}} \quad (J \text{ plate}), \\
 v_5 &= I_{\text{peak}}/I_{\text{tot}} \quad (F \text{ plate}), & v_6 &= I_{\text{peak}}/I_{\text{tot}} \quad (J \text{ plate}), \\
 v_7 &= A_3/A_{\text{tot}} \quad (F \text{ plate}), & v_8 &= A_3/A_{\text{tot}} \quad (J \text{ plate}), \\
 v_9 &= e \quad (F \text{ plate}), & v_{10} &= e \quad (J \text{ plate}),
 \end{aligned} \tag{1}$$

Here, A_{tot} is the total area of the image, A_3 the area within the third faintest areal profile, I_{tot} the total image density on the plate, I_{peak} the peak plate density, σ_{rr} the second radial moment, and e the image ellipticity.

Following image classification, the next step in the plate reduction was the calibration of photographic density in terms of the incident intensity on each plate. In order to accomplish this, a stellar-profile-based autocalibration technique similar to that described by Bunclark and Irwin (1984) was employed. This procedure worked as follows. Using the assumption that the density-to-intensity relationship near the sky was linear, the two faintest areal profiles of each star were used to obtain an estimate of $dr/d \log I$ at the radius corresponding to the mean of those isophotes. A least-squares cubic spline was then

fitted to these data points, and the resulting function integrated to obtain the plate point-spread function, $I_0(r)$. The relative intensities of the areal profile density levels, I_i , along with the stellar luminosities, L , were then calculated by iteratively solving the equation

$$\log L = \log L_0 + \log I_i - \log I_0(r_i). \quad (2)$$

Figure 2 presents a comparison of stellar magnitudes derived by this method with photoelectric photometry performed for the Space Telescope's Guide Star Selection System (Sturch *et al.* 1984; Lasker 1985). Despite the fact that a color transformation was needed to convert the B and V magnitudes to J and F , agreement between the photographic and photoelectric magnitudes is excellent, with no systematic errors apparent.

After solving for the plate calibration, galaxy magnitudes and colors were calculated by simultaneously fitting the areal profiles of both plates. This was done by first converting the measured areas into semimajor axis radii, r_i , and then computing the least-squares solution to the coupled equations

$$\begin{aligned} I_i &= c_0 + c_1 r_i^{1/4} + c_2 r_i + c_3 r_i^2 & (J \text{ filter}), \\ I_i &= c_0 + c_1 r_i^{1/4} + c_2 r_i + c_3 r_i^2 + C & (F \text{ filter}), \end{aligned} \quad (3)$$

where each point was weighted by the total intensity within its annulus, and C represents the galaxy's true color. An isophotal J magnitude for the galaxy was then found by integrating equation (3) out to some faint magnitude.

Implicit in this technique are two assumptions: that the $J - F$ color gradient within most galaxies are unimportant, and that the point-spread functions (PSFs) of the two plates being compared are similar. For the surface brightness being considered ($M_J \sim 21$) the first assertion seems to be true—most galaxies show no strong color change within their bright, central regions, and the few that do are almost always faint ($M_V > -22$; Strom and Strom 1978). For purposes of this study, the second assumption is also true. Although the detailed PSF of each plate is unique, because most of the plate pairs were taken one right after the other under nearly identical conditions, the variations in the PSFs are all small. The simultaneous fitting procedure described above was therefore

an excellent method of obtaining both galaxy magnitudes and colors with minimal errors.

To place the photographic magnitudes on an absolute scale, a two-step process was again employed. First the absolute J and F magnitudes from one late-type SAO star on each plate were obtained using single-channel photometer observations from Kitt Peak's 1.3 m telescope and several Landolt (1983) standard stars. These SAO stars then became JF system standards and were used to calibrate RCA CCD frames taken of ~ 50 faint ($m_J \gtrsim 17$) field galaxies. For the J filter, these CCD frames were obtained with the 1 m telescope at the Wise Observatory, Israel; for the F filter the observations came from both the Wise 1 m and the Kitt Peak No. 1 0.9 m telescope. By calibrating CCD frames containing photographically observed galaxies with frames of bright photoelectric standards taken through identical airmasses, the lowest intensity levels of the photographic plates were tied into the standard system.

III. GALAXY COUNTS

The most direct way of examining the quality and completeness of the wide-field photographic data is through galaxy number counts. Three corrections, however, had to be applied before the magnitudes calculated above could be used for analysis.

Preliminary plots of the raw differential galaxy counts versus magnitude showed a flattening of the power-law index at magnitudes $m_J < 17$. This proved to be due to the inclusion of blended star images as galaxies. Rather than forcibly trying to identify these misclassifications, a statistical method was adopted to remove the contamination. First the stellar size as a function of magnitude was recorded for each plate. Since this quantity was a by-product of the density-intensity autocalibration (cf. § II) the relation was easily accessible and well known. Next, the expected stellar color and luminosity functions for each field were estimated using the Bahcall and Soneira (1980, 1981a) model for the Galaxy. The probability of finding two stars with $\Delta m \leq 3$ at any given distance was then calculated, using the assumption that the nearest-neighbor distribution for stars fainter than $m_V > 16$ is not far from Poissonian (Bahcall

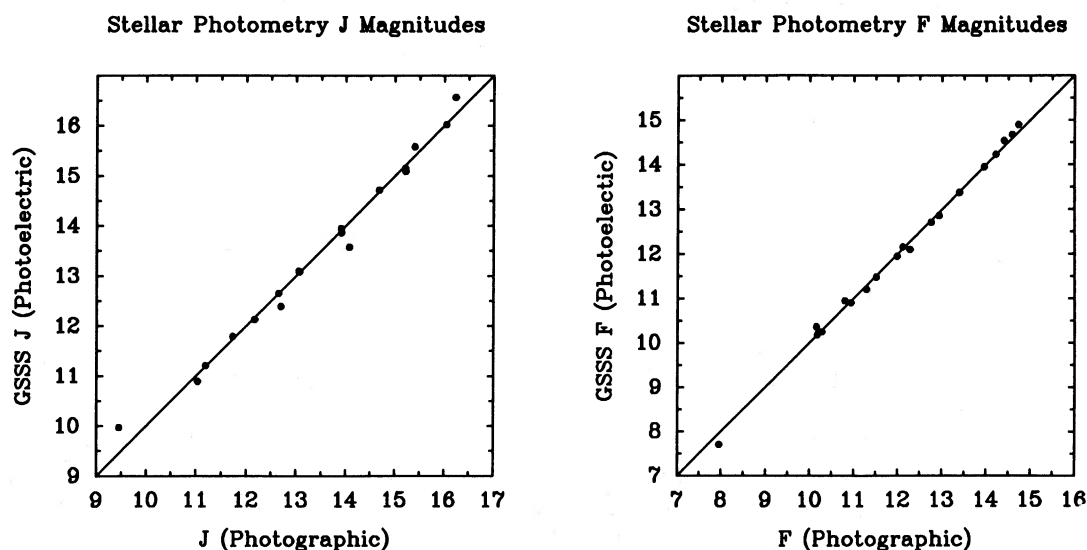


FIG. 2.—Space Telescope's Guide Star Selection System photoelectric photometry (Sturch *et al.* 1984), converted to the JF system, plotted against the image-profile-based photographic J and F magnitudes. Two stars with $m_J < 9$ have been omitted from the plot. The J -magnitude dispersion is $\sigma(J) = 0.22$ mag, while the F scatter is $\sigma(F) = 0.11$ mag.

and Soneira 1981*b*). Finally, from these probabilities, the number and color distribution of misclassified star blends were found by estimating the number of merged stellar images with $\Delta m \leq 3$ and assuming that the total luminosity and color of any blend was the sum of its individual components. This technique successfully corrected the $(\log N, m)$ -diagrams and resulted in a single power-law slope in each field.

Because the supercluster and both control fields are located at $\sim 62^\circ$ Galactic latitude, the interstellar extinction in these regions is expected to be small, and the differential reddening almost negligible. The Burstein and Heiles (1982) 21 cm radio maps show virtually no emission in the directions of interest, while the mean reddening laws of Sandage (1973), Burstein and McDonald (1975), and de Vaucouleurs, de Vaucouleurs, and Corwin (1976) give $E(B-V) = 0.00, 0.02,$ and $0.06,$ respectively. However, since a small uncertainty in the reddening translates into a substantial error in total extinction, an independent method was used to find the mean reddening in the fields.

Cluster surveys by CFBH, Ulrich (1978), Peterson (1978), Hoessel, Gunn, and Thuan (1980), and Schneider, Gunn, and Hoessel (1983) have recorded 56 galaxy redshifts in the three supercluster and two control fields. The $J-F$ colors of these galaxies are plotted against redshift in Figure 3 and compared with the expected K -corrected color of E and S0 galaxies. Points lying below (blueward) of the E/S0 curve in this color-redshift diagram can be attributed to later type galaxies; the systematic trend above this line, however, can only be due to interstellar reddening. A value of $E(J-F) = 0.045$ or $E(B-V) = 0.03$ was therefore adopted in both the supercluster and control fields, and the galaxy magnitudes and colors were corrected accordingly.

The final correction applied to the galaxy counts was a deconvolution of the effects of random observational errors. To estimate this effect, the CCD magnitudes of the photometric reference galaxies of § II were compared with their calculated Schmidt plate magnitudes, and the scatter as a function of magnitude was computed. Based on these results, a constant observational error of $\sigma \approx 0.10$ mag was adopted for all galaxies brighter than $m_J = 18$; for fainter galaxies, the error term

was increased until it reached $\sigma \approx 0.28$ mag at $m_J \approx 21$. The galaxy counts were then corrected using these error estimates and the Taylor series expansion for a deconvolution with a variable width filter (Trumpler and Weaver 1953).

Figure 4 displays in 0.5 mag bins the corrected differential galaxy counts in each of the five Schmidt fields. One obvious feature of the counts is the variability in the number of galaxies in each field. Part of this may be due to errors in the magnitude zero point of each plate, since this relies solely on the CCD photometry of faint galaxies. However, a more probable explanation is that the galaxy counts fluctuate from field to field, as the discrepancies between the counts of several authors suggest (cf. Shanks *et al.* 1984). This view is supported by the fact that the galaxy counts for all three supercluster Schmidt fields lie above those of the control fields at just those magnitudes where the contribution from the rich supercluster is expected to be important. Interstellar extinction cannot be invoked to explain this phenomenon, since the mean differential extinction between the supercluster and the control fields must be small, and any patches of Galactic dust, such as those suggested by the *IRAS* infrared cirrus observations (Low *et al.* 1984), cannot affect the counts over an area as wide as a 22 square degree Schmidt plate.

Figure 5 compares the fully corrected J filter differential galaxy counts averaged over the five Schmidt fields with the counts found by other authors in the B_J bandpass. The data are again binned in 0.5 mag intervals. Although the color passbands are not quite identical, there is extremely good agreement for all but the counts of Shanks *et al.* (1984). The best fit for the mean of these five field counts is

$$\log N = (-6.78 \pm 0.14) + (0.45 \pm 0.01)m_J. \quad (4)$$

The best fit for the central 4° of the supercluster 1451+22 is

$$\log N = (-6.58 \pm 0.30) + (0.44 \pm 0.02)m_J, \quad (5)$$

while the fit to the control fields yields

$$\log N = (-6.66 \pm 0.23) + (0.44 \pm 0.01)m_J. \quad (6)$$

The data in all the fields are complete to past $m_J = 20.5$.

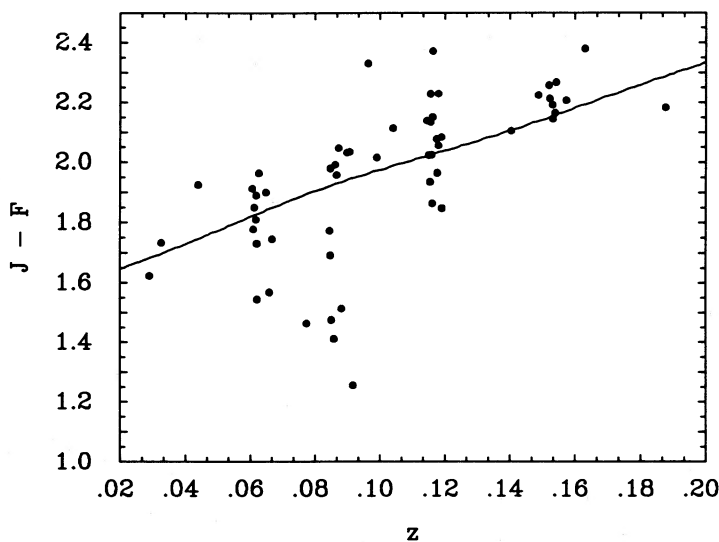


FIG. 3.—Observed color-redshift relation for all galaxies with known redshifts in both the supercluster and the control fields. The solid line represents the JF system theoretical relation for ellipticals. The data imply that a small amount of reddening [$E(B-V) = 0.03$] exists in the fields.

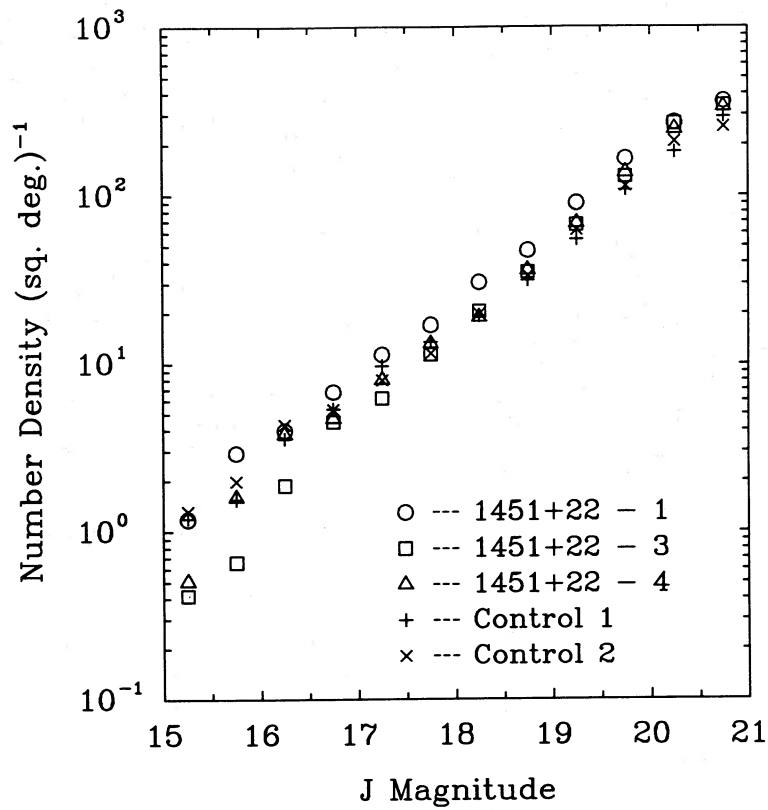


FIG. 4.—Corrected differential galaxy counts in the J filter for each Schmidt field. The data have been binned into 0.5 mag intervals and are complete past $m_j > 20$.

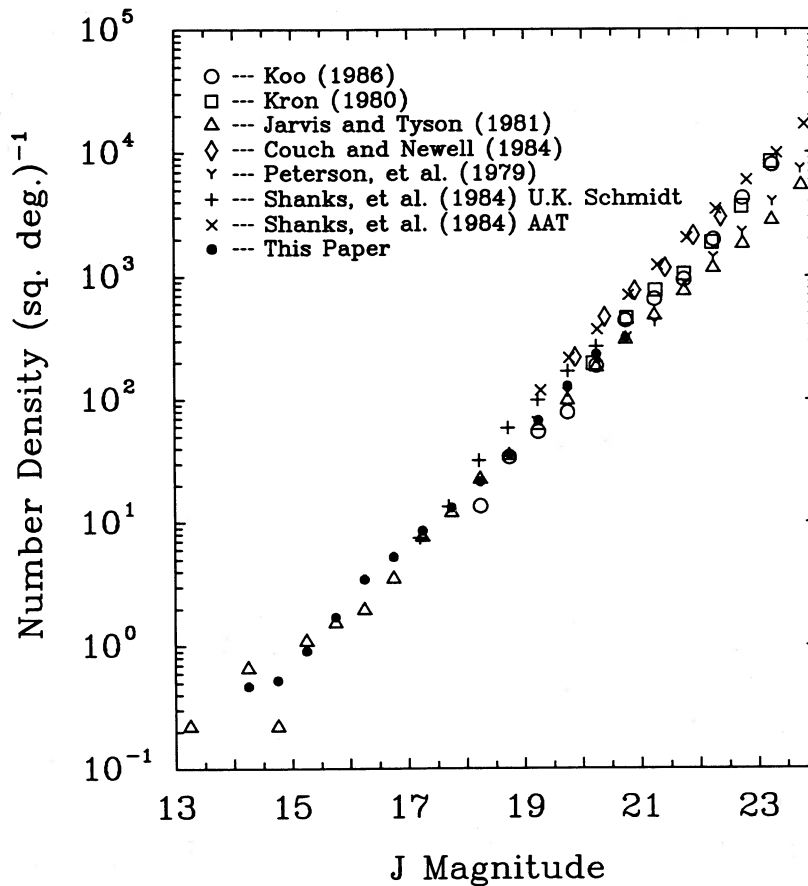


FIG. 5.—Mean differential J -magnitude counts for the five Schmidt fields, binned into 0.5 mag intervals and compared with the counts of other authors. The data agree very well with all but the counts of Shanks *et al.* (1984).

IV. THE SUPERCLUSTER'S EARLY-TYPE GALAXIES

Since the apparent colors of galaxies change with redshift, as spectral continuum features move through the filter bandpasses, a color-redshift relation exists for all galaxies. In particular, elliptical and S0 galaxies at a given redshift occupy a specific location in the color-magnitude diagram (Sandage 1973; Butcher *et al.* 1976). Therefore, when viewed in the appropriate color band, the majority of background and foreground galaxies disappear, leaving only the E and S0 galaxies at the redshift of interest. The theoretical color-redshift relations for the JF system are shown in Figure 6. Although elliptical galaxies at the redshift of the supercluster ($z \approx 0.11$) have the same color as Sab galaxies at $z \approx 0.22$ and Sbc galaxies at $z > 0.37$, because these later type galaxies are much more distant, their effect on a color-selected sample is minimal. Cosmic color scatter is important, since it tends to blur out the color-redshift relation, but since superclusters have a high density contrast in redshift space compared with their surroundings (cf. Oort 1983 and references therein), contamination by early-type galaxies immediately in front of or behind the supercluster is also small. Hence it is possible to trace the morphology of a supercluster through the probable identification of supercluster ellipticals based on color.

Figure 7 is a luminosity contour map of 1451+22 formed from only those galaxies likely to be elliptical or S0 galaxies in the supercluster (i.e., with $m_J > 17$ and $1.95 < J - F < 2.15$). Several points are immediately noticeable from the figure. First, all of 1451+22's Abell clusters are easily recognizable, with the centrally located, richness class 1 cluster Abell 1986 being the most prominent. The CFBH small groups are also visible, though many are not obvious. The redshift discrimination is not perfect, however, since the nonmember richness class 1 clusters Abell 1939 (a $z \approx 0.088$ enhancement in the extreme northwest section of the map) and Abell 2009 (the linear structure east and slightly south of center at $z \approx 0.153$) are also apparent.

Another feature visible through the contour map is the

degree of filamentary structure exhibited by the supercluster. Abell 1972, 1980, and 1986 appear connected in a stream of elliptical galaxy luminosity extending $18h^{-1}$ Mpc outward from the center at a position angle of 330° . Although the plates do not cover the area, it is probable that this structure (hereafter called the primary filament) extends down to Abell 1988 as well. Abell 2036, a richness class 0 cluster which lies $\sim 40h^{-1}$ Mpc from the supercluster center in the southeast corner of the map, is *not* part of this filament, however. In fact, despite the fact that it is roughly in line with the primary filament, the absence of luminosity surrounding this cluster argues against its being associated with 1451+22 at all.

Even though the primary filament may be an important part of the supercluster, it is not overwhelming, and much of 1451+22's luminosity is not in this cloud. Abell 1976 lies perpendicular to the structure in the southwest quadrant of the supercluster, while Abell 2001 is northeast of center in the region not surveyed. (The position angle of the linear cluster Abell 1986 is also perpendicular to the primary filament and in line with this secondary axis.) In addition, there are many CFBH groups in the northeast and western portions of the field which have no connection to either filament.

In order to search for evidence of a density fall off with radius, galaxies with colors in the range $1.95 < J - F < 2.15$ and magnitudes $16.5 < m_J < 20.5$ were counted in $15'$ thick circular annuli centered on the rich cluster Abell 1986. To estimate the background, counts in this same bandpass were performed on the two control fields. Figure 8 shows the results of these counts. The supercluster is clearly visible, since the mean number density of E/S0-like galaxies in the region is always greater than 60, whereas this number is only 45 for control field 1 and 56 for control field 2. Except for an increase in the very center of the supercluster (an area dominated by Abell 1986), however, there is only slight evidence for a radial gradient in the number density of E and S0 galaxies. Ignoring the central degree, a formal least-squares line through the data yields a barely significant decreasing slope of 0.038 ± 0.026 .

The galaxy enhancement in the primary filament was inves-

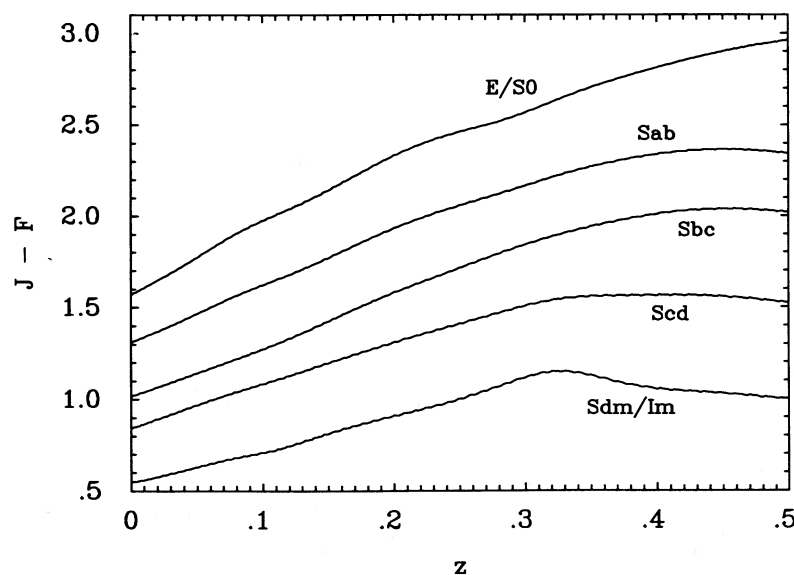


FIG. 6.— $J - F$ colors of galaxies of types E/S0, Sab, Sbc, Scd, and Sdm/Im as a function of redshift. The figure reflects the action of the K -correction only; evolutionary effects are ignored. The curves for all but the Sab galaxies are based on the data of Coleman, Wu, and Weedman (1980). The Sab galaxy curve is a combination of E/S0 and Sbc curves, normalized to the optical energy distribution of Pence (1976).

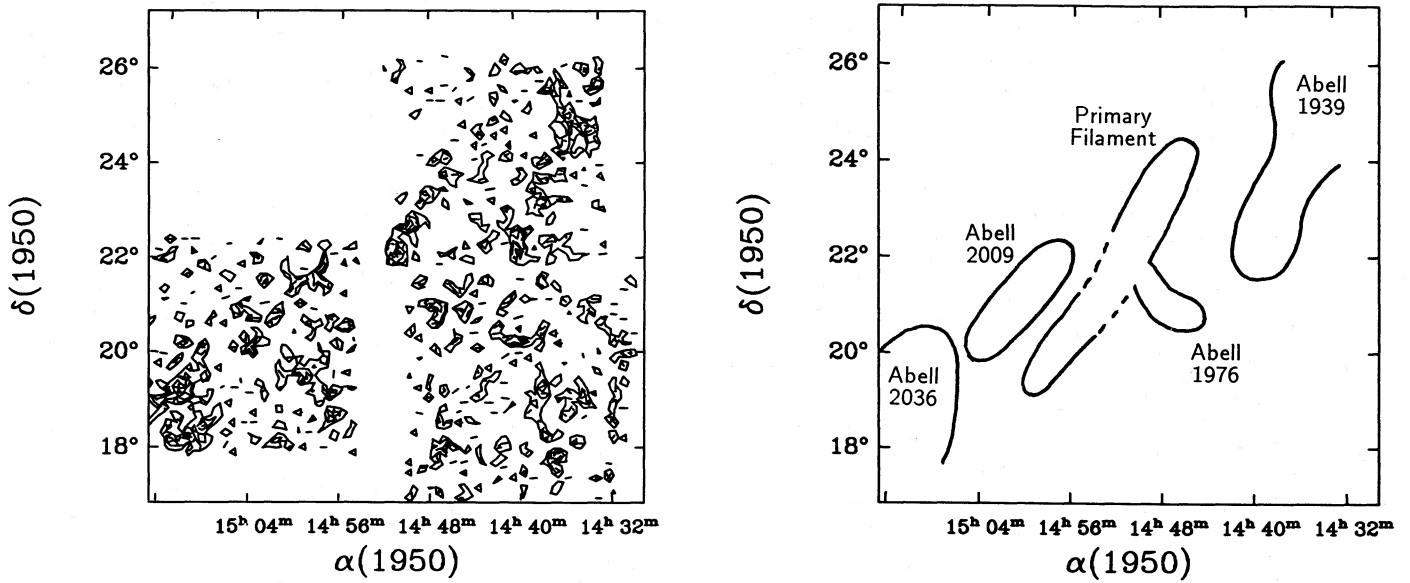


FIG. 7.—Contour plot of luminosity emanating from galaxies with a $J-F$ color in the range $1.95 < J-F < 2.15$. At the redshift of the supercluster, this range corresponds to the color of normal elliptical and S0 galaxies. Panel *a* contains the data binned into regions $6/24$ square in size. The primary filament can be seen extending from the supercluster center at a position angle of 330° . The long thin filament east and slightly south of center is Abell 2009 at $z \approx 0.153$. In the extreme southeast corner is Abell 2036. A system at $z \approx 0.088$ which includes Abell 1939 and several CFBH groups can be seen extending south-southeast from the northwest corner of the field. These features are diagrammed in panel *b*.

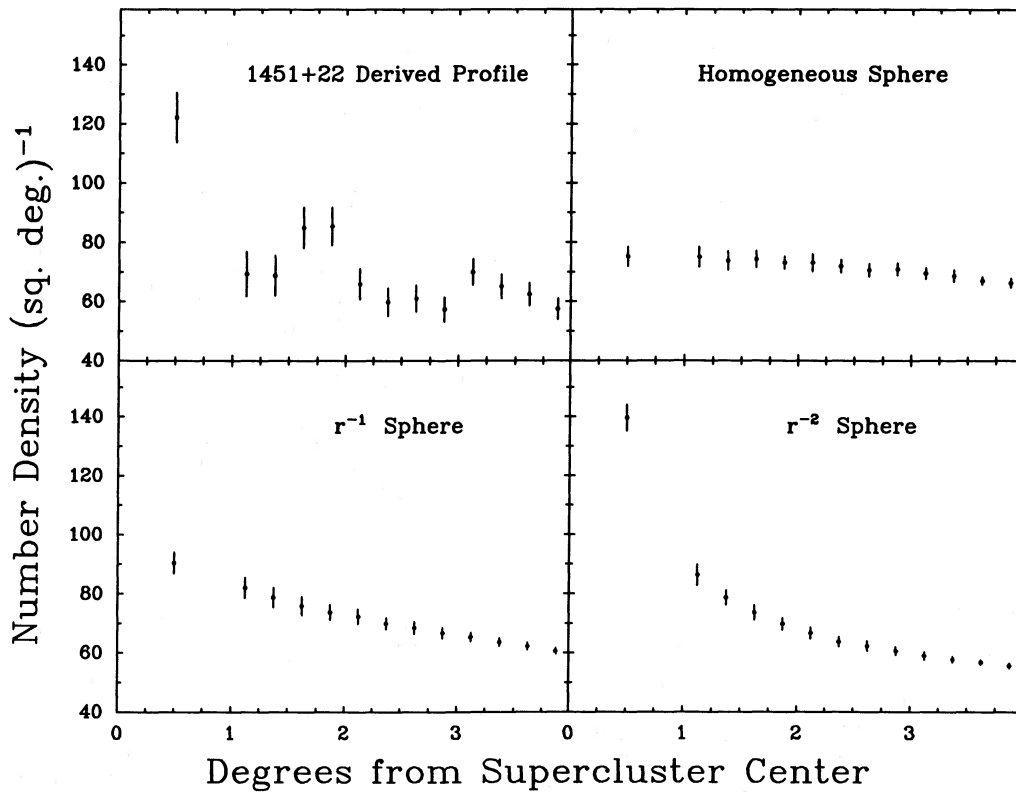


FIG. 8.—Number density of galaxies with a magnitude in the range $16.5 < m_j < 20.5$ and the color of supercluster ellipticals plotted against distance from the center of the supercluster, and compared with spherically symmetric models. The annuli are $15'$ thick, except for the central region, which extends 1° outward. The error bars on the observed points represent counting statistics only. As a comparison, the number density of galaxies in this color-magnitude region is 45 galaxies per square degree in control field 1 and 56 in control field 2. The spherically symmetric models do not fit the observations well.

tigated in a similar manner. E/S0 galaxy counts were performed on a series of 0.5° wide strips extending from the center of the supercluster out to a radius of 2.5° . The results of these counts, with the central Abell cluster 1986 excluded, are plotted against position angle in Figure 9. The primary filament is easily identified through the density enhancement at the position angle of 150° , but a substantial number of galaxies exist outside this structure. If we assume that the control field background density of ~ 50 also applies to the field of 1451 + 22, the enhancement of elliptical and S0 galaxies in the primary filament is $\sim 40\%$ over neighboring regions. Much of this overdensity can be attributed to the Abell clusters which define the structure.

a) Percolation Tests

The statistical analysis of shape is not very well developed, and although several tests for filaments do appear in the literature (e.g., Moody, Turner, and Gott 1983; Kuhn and Uson 1982), most can be fooled by certain types of galaxy distributions, and none are completely satisfactory. Percolation theory is perhaps the best known and most popular method of analyzing linear structures (Zel'dovich, Einasto, and Shandarin 1982), so this type of test was applied to the supercluster elliptical galaxy data.

The test formulation used was that of Bhavsar and Barrow (1983). A single-connection or "friends of friends" clustering algorithm was run on the surface distribution of the probable supercluster ellipticals. For each field, the dimensionless parameter L , defined as the length of the longest galaxy chain divided by the size of the region, was plotted against the linking radius r , expressed in terms of the projected mean intergalaxy distance. In such a diagram a population of objects drawn from primarily linear distributions will yield a curve which exponentially increases at the critical linking radius $r \approx 0.7$ (Hammersley and Welsh 1980). Figure 10 displays the observed curves for the five Schmidt fields, along with the

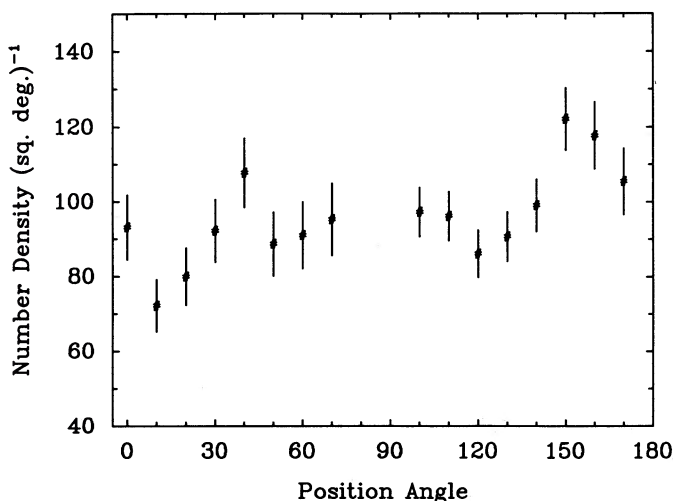


FIG. 9.—Number density of galaxies with a magnitude in the range $16.5 < m_r < 20.5$ and the color of supercluster ellipticals plotted against the position angle of an axis through the center of the supercluster. The counts, binned into 10° azimuthal sections, include only those galaxies within 2.5° of the supercluster center and outside Abell 1986, as defined by Abell (1982). The error bars displayed are from counting statistics only. Assuming a background number density of 50, the primary filament at position angle 150° has $\sim 40\%$ more elliptical galaxies than its neighboring regions.

range of values expected from an underlying Poissonian distribution. Although the data for each field are somewhat indicative of linear structures, the slope is not great enough to rule out purely random distributions. Percolation tests therefore do not appear to be a sensitive shape discriminant for this kind of data.

V. GALAXY COLOR-MAGNITUDE DIAGRAM

The variations in the galaxy counts in any given color-magnitude range reflect both real fluctuations in the space density of galaxies and shifts in the mix of galaxy morphological types. For example, rich clusters have more E and S0 galaxies than the field, and therefore have a greater population of red objects. In addition, in at least one linear supercluster, Perseus, a partial segregation by galaxy type has been observed to occur (Giovannelli, Haynes, and Chincarini 1986). In order to disentangle the population effects from the density measurements, theoretical galaxy color-magnitude diagrams were calculated and compared with the observed diagram for supercluster and control fields.

To do this, galaxies were divided into five spectral classifications, E/S0, Sab, Sbc, Scd, and Sdm/Im, and three Schechter (1976) luminosity functions were adopted for each (cf. Table 2). Using the energy distributions of Coleman, Wu, and Weedman (1980) and the filter transmission curves of Figure 1, the color-redshift relation for each class was calculated, and a 0.12 mag cosmic scatter in color, similar to that observed by de Vaucouleurs and de Vaucouleurs (1972) added. Theoretical color-magnitude diagrams for the control fields were then computed by varying the mix of galaxy types and the universal luminosity density until a maximum-likelihood condition between theory and observations was reached. The supercluster fields were modeled in a similar fashion, using the control field representations as an estimate of the field galaxy contribution.

a) Control Fields

Table 3 lists the best-fitting galaxy mixes and luminosity densities for the two control fields. A variation of the Schechter cutoff magnitude M^* with galaxy type similar to that found by Ellis (1982) and King and Ellis (1985) was considered in the models labeled A; in the B models this relation was flat (as explored by Shanks *et al.* 1984), while in the C models the variation was extreme (similar to that suggested by Tammann, Yahil, and Sandage 1979). No fit was perfect, although the *observed minus calculated* residuals, binned into intervals 0.25 mag wide in magnitude and 0.05 mag in color, were never more than a few percent. In general, the models suffered from three minor shortcomings.

TABLE 2
SCHECHTER PARAMETERS FOR MODELS ($H_0 = 50 \text{ km s}^{-1} \text{ Mpc}^{-1}$)

GALAXY TYPE	MODEL A ($\alpha = -1.05$)		MODEL B ($\alpha = -1.25$)		MODEL C ($\alpha = -1.05$)	
	M_J^*	$M_{B_i}^*$	M_J^*	$M_{B_i}^*$	M_J^*	$M_{B_i}^*$
E/S0	-20.70	-20.96	-21.00	-21.26	-21.00	-21.26
Sab	-20.60	-20.78	-21.00	-21.18	-20.50	-20.68
Sbc	-20.45	-20.56	-21.00	-21.11	-20.00	-20.11
Scd	-20.30	-20.38	-21.00	-21.08	-19.50	-19.58
Sdm/Im	-20.15	-20.18	-21.00	-21.03	-19.00	-19.03

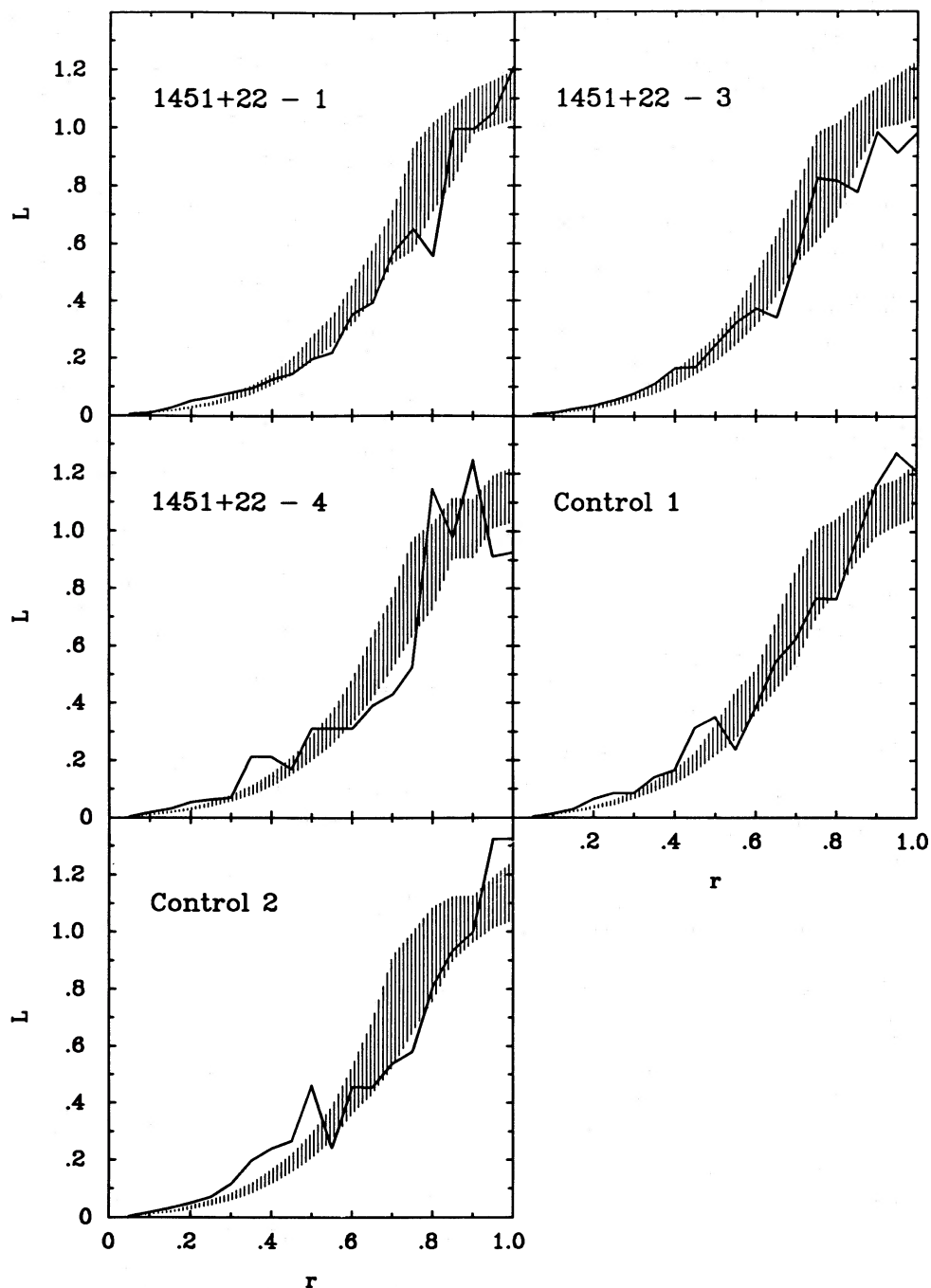


FIG. 10.—Results of percolation tests applied to those galaxies in the supercluster and control fields which have the colors of supercluster ellipticals. The abscissa is a dimensionless distance in terms of the mean interparticle distance. The ordinate is the longest linear extent of any association divided by the size of the Schmidt field. The lines are the percolation curves for each field; the shaded region is the 1σ variation found from 100 Monte Carlo simulations of particles drawn from a Poissonian distribution. Although the curves percolate to some extent, in none of the cases is the evidence for filamentary structure compelling.

1. The computed models underestimated the number of galaxies with extreme colors. In both the red and the blue, the models cut off faster than the observed distribution, especially for moderately bright galaxies. Object blends and plate flaws provide a natural explanation for this. Because the effects of image contaminants are different from plate to plate, the colors of objects with these problems are extreme. In addition, since there are few bright galaxies, a small population of objects with ill-determined magnitudes yields a relatively large percentage

error. These errors could not be removed with first-order error theory, since the underlying magnitude distribution is clearly non-Gaussian.

2. All the models overestimated the number of blue galaxies in the range $18 < m_J < 19$. A detailed examination showed, however, that this discrepancy was a property more of the control fields than of the models. Both control fields contain a true dearth of blue galaxies at these magnitudes, to the extent that the $d \log N/dm$ relation for blue galaxies nearly contains

TABLE 3
BEST MODELS FOR THE CONTROL FIELDS

MODEL	OBSERVED GALAXIES ($m_J < 16.5$)					$\mathcal{L}/L_{J_{\odot}^{-3}}$ ($h \text{ Mpc}^{-3}$)
	E/S0	Sab	Sbc	Scd	Irr	
Control Field 1						
A.....	0.26	0.21	0.38	0.13	0.02	1.4×10^8
B.....	0.25	0.23	0.31	0.18	0.03	1.4×10^8
C.....	0.27	0.33	0.29	0.10	0.01	1.4×10^8
Control Field 2						
A.....	0.32	0.27	0.37	0.03	0.01	1.6×10^8
B.....	0.29	0.26	0.40	0.03	0.02	1.6×10^8
C.....	0.30	0.34	0.34	0.01	0.01	1.7×10^8
Control Fields 1 and 2 Combined						
A.....	0.32	0.23	0.36	0.07	0.02	1.6×10^8
B.....	0.27	0.24	0.37	0.08	0.04	1.5×10^8
C.....	0.27	0.38	0.28	0.05	0.02	1.6×10^8

an inflection point. This may be a local anomaly, possibly caused by the influence of the Local Supergalactic plane on the galaxy population, and in terms of total numbers of galaxies the effect is not severe. Although the percentage deviation from the models is highest in this region of the color-magnitude diagram, sometimes reaching 7%, the addition of ~ 10 galaxies would more than make up for the deficiency.

3. The models as a rule underestimated the number of faint blue galaxies by a couple of percent. In part this was due to the absence of the brighter blue galaxies—obviously it is difficult to simultaneously adjust the number of galaxies at $m_J \sim 20$ up and the number at $m_J \sim 19$ down. However, an additional effect might have caused the observations to fall short of the models. The blue galaxies in this section of the diagram are the faintest recorded on both the J and the F plates. Care was taken to see that the sample was complete; however, if the errors associated with the faintest magnitude measurements were underestimated, the true number of galaxies would have been overestimated. Also, in this section of the diagram the measurement error is changing very rapidly with magnitude—possibly too rapidly for the first-order corrections which were applied. An overestimate of the true galaxy density would again be the result.

After these “universal” problems were identified, the properties of the individual fits were analyzed. First, and perhaps most disconcerting, were the differences observed between the two control fields. Although control field 2 contains more galaxies than control field 1, the fraction of blue galaxies in it appears to be much smaller. Because this field does not contain any galaxies with measured redshifts, it is possible (though unlikely) that a difference in the Galactic reddening or an error in the zero-point calibration could be the cause. Significantly, however, the fits for the two control fields combined are better than those for the individual fields, suggesting that at the magnitudes under consideration, fluctuations on scales as large as a Schmidt plate do exist. (This, in fact, should not be too unexpected, since at $m_J \sim 20$ the mean redshift of a sample of galaxies is $z \sim 0.15$, a distance at which a $40h^{-1}$ Mpc size supercluster extends 5° on the sky.)

A second feature of the models is the small number of late-type galaxies. The models for the two control fields combined imply that less than 15% of the galaxies in the sky brighter

than $m_J = 16.5$ are Scd and Sdm/Im. This is somewhat lower than that found by the various surveys (cf. Table 4 in Ellis 1982), but not by an extraordinary amount. Several effects might contribute to this discrepancy. First, as already noted, both control fields have a significant underabundance of blue galaxies at $m_J \sim 19$. This dearth of galaxies affects the fits and brings down the derived number of late-type galaxies. If the calibration or Galactic reddening of control field 2 is incorrect, an increase in the percentage of blue galaxies might also be the result. Finally, the observed mix of morphological types for bright galaxies is biased by contamination from the Local Supercluster. Since the volume of space sampled in this color survey is larger than that of the morphological surveys, the derived fraction of blue galaxies may be different.

Despite these small inconsistencies, the models fit the observed galaxy color-magnitude diagram very well, the worst discrepancies are always of the order of a few percent, and the observables predicted by the models are reasonable. The Ellis (1982) variation of M^* with galaxy type (model A) is slightly better than the flat or steep relations of models B and C; the mix of galaxy types, even with the scarcity of blue galaxies, is not too different from that observed; and the values for the luminosity density, \mathcal{L} , are very close to those found by other authors (Table 4). This agreement was deemed good enough to allow the control fields to be used as estimates of the field galaxy density of the supercluster.

b) Supercluster Models

The observed color-magnitude diagram for 1451+22 contains galaxies both in and out of the supercluster. In order to measure just the supercluster, the contribution from the field was first removed. This was done by simply subtracting the theoretical color-magnitude diagrams obtained from the control fields from those observed from the supercluster fields. To gain some idea of the uncertainty involved in this, three different subtractions were performed: one using control field 1 as the field estimator, one using control field 2, and one using the combined control fields. After the background subtractions, the remaining data were fitted in a manner similar to the control fields, with the integration restricted over the redshift range of the supercluster.

To measure the radial profile of 1451+22, the supercluster was divided into a series of 1° thick concentric rings centered on Abell 186. For each annulus the supercluster contribution to the galaxy surface density was modeled and the variation of \mathcal{L} and galaxy content with radius calculated. Although the precise values varied somewhat with the presumed Schechter functions and field galaxy contribution (i.e., the dearth of blue galaxies in control field 2 propagated directly into a higher proportion of late-type galaxies in the supercluster), the overall

TABLE 4
OBSERVED GALAXY LUMINOSITY DENSITIES

Reference	$\mathcal{L}/L_{J_{\odot}^{-3}}$ ($h \text{ Mpc}^{-3}$)
Schechter 1976	4.6×10^8
Felten 1977	2.4×10^8
Huchra 1978	2.7×10^8
Davis, Geller, and Huchra 1979	1.7×10^8
Kirschner, Oemler, and Schechter 1979	1.8×10^8
Ellis 1982	8.8×10^7
This paper	1.5×10^8

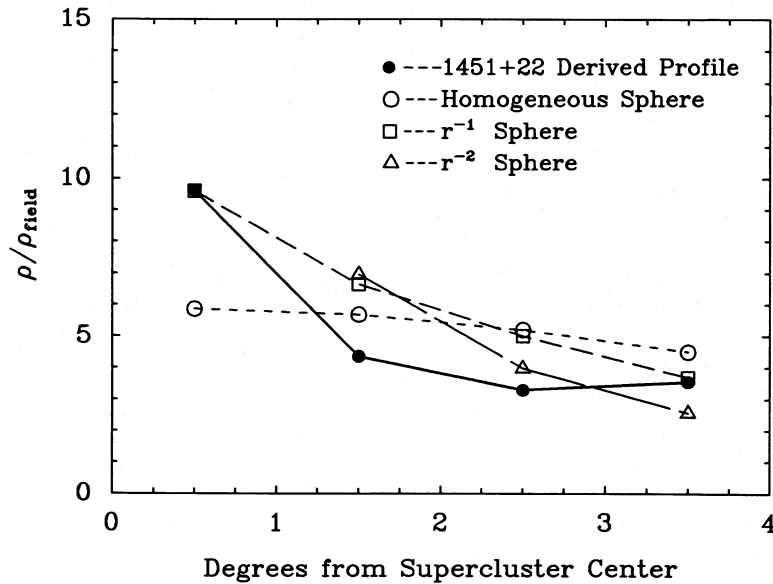


FIG. 11.—Radial luminosity density contrast of the supercluster field for model A Schechter parameters and the combined control field background plotted with the spherically symmetric supercluster models. The data are binned into 1° intervals. The values of the density contrast assume the volume calculated for a spherical supercluster; these can be scaled by a factor of 1.75 to obtain the values for a flat system. None of the spherically symmetric models is a good fit to the data.

supercluster properties are largely model-independent. In general, the A models, which used the Ellis (1982) M^* variation with galaxy type, provided the best fits, while the fits obtained using model C's steep variation of M^* with morphological type were uniformly poorer.

Figure 11 presents the variation of \mathcal{L} with radius found using the model A parameters and the combined control fields. Figure 12 shows the radial change in supercluster galaxy mix for the same model. Immediately noticeable is the very small variation with radius in the outer portions of the supercluster. In the central 1° , where Abell 1986 dominates, the galaxy density is high, and the proportion of galaxies is strongly

skewed toward the early-type galaxies. The density drops significantly between 1° and 2° , however, as does the percentage of ellipticals. Once past this point, the decrease of galaxy density with radius is small, and the mixing of galaxy types becomes that of the field. While this profile does not resemble that of a projected spheroid, it is suggestive of a core-halo morphology, where a central concentration of galaxies, which includes five Abell clusters, is surrounded by a diffuse halo.

Using the same modeling technique, the galaxy enhancement in the primary filament was also investigated. Two $30'$ wide strips extending $2.5'$ out from the supercluster center were selected for study, one centered on the primary filament at position angle 150° and one positioned 20° away at position angle 130° . Once again, the results were independent of the precise details of the model: a galaxy's azimuthal position in 1451+22 is very important in determining its environment. The primary filament has a $\sim 40\%$ luminosity density enhancement over its surroundings, a value which agrees with that found in § IV. Coupled with this enhancement is a population shift toward the early-type galaxies. The fraction of elliptical, S0, and Sab galaxies in the filament is $\sim 10\%$ greater than that in other regions of the supercluster, while the proportion of Scd and Sdm/Im galaxies is down by an equal amount. This result can be compared with that from the radial data, which shows no change in the galaxy population once outside the central degree.

Not all this enhancement is due to the rich clusters. The analysis of color-magnitude diagrams made from the on-filament $5^\circ \times 0.5'$ strip with the Abell clusters removed shows that even without these clusters, this region contains more luminosity and a higher percentage of early-type galaxies than do the off-filament fields. When all the galaxies within the regions defined by Abell (1982) are excluded, there is still a $\sim 5\%$ enhancement in the fraction of elliptical, S0, and Sab galaxies, and a 10%–20% excess in the luminosity density.

As important as the primary filament is, two things must be kept in mind when interpreting these data. First, while the above properties are interesting, they are not unexpected. The

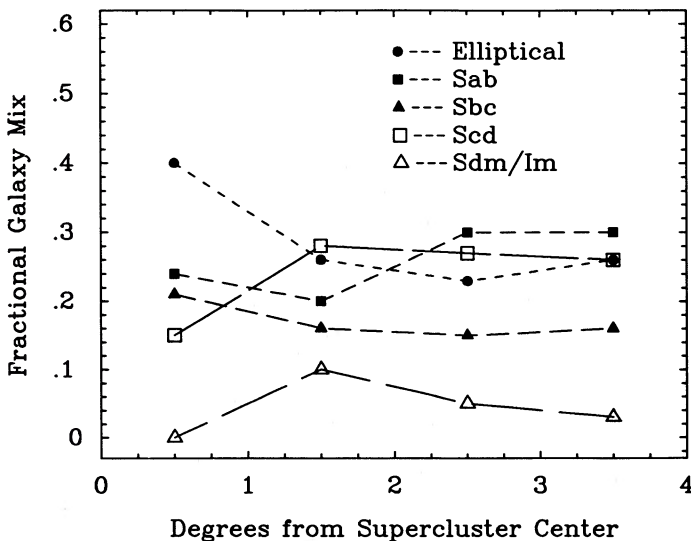


FIG. 12.—Fraction of galaxy morphological types vs. distance from the supercluster center for model A Schechter parameters and the combined control field background. The data are binned into 1° intervals. In the central 2° , the percentage of early-type galaxies decreases with radius. Outside this region, there is no significant gradient in any of the morphological classifications.

primary filament is formed out of, and in truth defined by, four Abell clusters, hence this region must have a high luminosity density and should contain a large fraction of early-type galaxies. If one considers the Abell clusters just as peaks in a smooth galaxy density distribution, then the regions between nearby Abell clusters must also have a higher than average galaxy density. (Bridges between rich clusters are not uncommon, the Coma/Abell 1367 stream being a good example.) Thus, even when the Abell clusters are excluded, the primary filament stands out. The filament does not dominate the entire supercluster, however. Since the total volume of the filament is small and the density contrast not overwhelming, the bulk of the supercluster's mass is still in the off-filament regions.

Two interesting quantities in the study of superclustering are the total mass contained in the supercluster, and the density contrast of the system. Although neither is measurable directly, both can be estimated through the models of the color-magnitude diagram.

The first step in estimating these quantities was to calculate the supercluster luminosity density, \mathcal{L} . To do this, the true supercluster volume was needed. In their redshift survey of 23 rich clusters and groups, CFBH measured a velocity dispersion of $\sigma(z) = 0.00188$ in the $\sim 8^\circ \times 5^\circ$ supercluster field. This can be transformed into a depth in two ways. If 1451+22 is modeled as a thin face-on pancake, the redshift dispersion can be translated into a physical thickness by taking 4 times the distribution's probable error, which yields a total volume for the supercluster slab of $\sim 20,000h^{-3} \text{ Mpc}^3$. If a quasi-spherical supercluster is preferred, no depth information is contained in the redshifts, but a volume of $\sim 35,000h^{-3} \text{ Mpc}^3$ can be inferred from the projected size.

Using these values for the supercluster volume, mean luminosity densities were then calculated from the supercluster models. Because the supercluster seems to exhibit a core-halo structure, two regions were defined: one including just the 2° supercluster core, and one extending 4° in radius, containing both the core and the halo. The best-fitting models and the luminosity densities derived from these regions are summarized in Table 5.

Once the supercluster luminosity densities were adopted, the density contrasts followed immediately. Each value for \mathcal{L} was divided by that obtained through the corresponding control field model, so that a series of self-consistent luminosity ratios were found. Assuming that the mass-to-luminosity ratio in the supercluster is similar to that of the control field, these luminosity ratios are equivalent to density contrasts. The derived values are presented in Table 6. For the central region of supercluster 1451+22, the density contrast is between 15 and 20 for the flat supercluster models and between 8 and 11 for the spherically modeled systems. For the region as a whole, the density contrasts are ~ 10 and ~ 6 , respectively. Both of these estimates are independent of the precise details in the fits. Although the values found for the flat supercluster are higher than those found for nearby systems, it must be remembered that 1451+22 is the richest supercluster studied to date, and therefore the large density enhancement is not unexpected.

Two other quantities obtainable from the luminosity density are the total J luminosity of the system and the total visible mass. For the luminosity, no further assumptions are required—the luminosity density \mathcal{L} is just multiplied by the volume of the supercluster. When this is done, of course, the assumptions about 1451+22's geometry divide out, leaving a number which is independent of the supercluster's thickness. All the models give a value of $\sim 6 \times 10^{13} h^{-2} L_{J_\odot}$ as the total luminosity of the supercluster.

The total mass estimate is also independent of geometry, but it does require a guess as to the mass-to-luminosity ratio for galaxies. Although some type of dark matter that is only detectable via dynamical studies probably dominates the mass of the system, it is possible to get a rough measure of the visible mass by using a mass-to-light ratio observed for the inner parts of galaxies. Estimates of M/L for the center of both early- and late-type galaxies all lie somewhere between 2 and 10 (Faber and Gallagher 1979). Hence a reasonable lower limit to the total mass of the supercluster can be obtained by multiplying the system's total luminosity by 5. This is done in Table 6. Independent of the model, the derived visible mass of 1451+22 is $\sim 3 \times 10^{14} h^{-2} M_\odot$. Roughly two-thirds of this mass lies

TABLE 5
BEST MODELS FOR THE INTEGRATED SUPERCLUSTER

MODEL	MIX OF MORPHOLOGICAL TYPES ($m_J < 16.5$)					CENTRAL 2° \mathcal{L}/L_{J_\odot} ($10^9 h$ Mpc^{-3})		ENTIRE SUPERCLUSTER \mathcal{L}/L_{J_\odot} ($10^9 h \text{ Mpc}^{-3}$)	
	E/S0	Sab	Sbc	Scd	Irr	Flat	Spherical	Flat	Spherical
Field Galaxy Estimate from Control Field 1									
A.....	0.33	0.33	0.20	0.13	0.02	2.6	1.5	1.8	1.0
B.....	0.37	0.33	0.16	0.11	0.03	2.8	1.6	2.2	1.3
C.....	0.39	0.32	0.19	0.06	0.04	2.8	1.6	1.8	1.0
Field Galaxy Estimate from Control Field 2									
A.....	0.24	0.18	0.15	0.32	0.11	2.3	1.3	1.4	0.8
B.....	0.22	0.20	0.11	0.34	0.12	2.3	1.3	1.5	0.9
C.....	0.30	0.16	0.11	0.32	0.12	2.2	1.3	1.8	1.0
Field Galaxy Estimate from Combined Control Fields									
A.....	0.26	0.28	0.16	0.23	0.06	2.3	1.3	1.6	0.9
B.....	0.27	0.28	0.09	0.31	0.06	2.2	1.3	1.7	1.0
C.....	0.32	0.27	0.11	0.22	0.08	2.7	1.5	1.9	1.1

TABLE 6
INTEGRATED SUPERCLUSTER PROPERTIES

MODEL	CENTRAL 2°				ENTIRE SUPERCLUSTER			
	$L/L_{J\odot 2}$ $10^{13}h^{\odot 2}$	M/M_{\odot} $10^{14}h^{-2}$	ρ_L/ρ_{Lfield} Flat	ρ_L/ρ_{Lfield} Spherical	$L/L_{J\odot 2}$ $10^{13}h^{\odot 2}$	M/M_{\odot} $10^{14}h^{-2}$	ρ_L/ρ_{Lfield} Flat	ρ_L/ρ_{Lfield} Spherical
Field Galaxy Estimate from Control Field 1								
A.....	2.2	1.1	19	11	6.3	3.1	13	7
B.....	2.4	1.2	20	11	7.5	3.7	16	9
C.....	2.4	1.2	20	11	6.0	3.0	12	7
Field Galaxy Estimate from Control Field 2								
A.....	1.9	0.97	14	8	4.7	2.3	8	5
B.....	1.9	0.96	14	8	5.1	2.5	9	5
C.....	2.2	1.1	15	9	6.3	3.1	11	6
Field Galaxy Estimate from Combined Control Fields								
A.....	2.0	1.0	14	8	5.4	2.7	10	6
B.....	1.9	0.96	15	9	5.7	2.8	11	6
C.....	2.3	1.2	16	9	6.4	3.2	11	6

outside the 2° supercluster core. Since most superclusters have been estimated to contain between 2×10^{14} and $10^{15}h^{-2} M_{\odot}$, any reasonable total mass-to-light ratio will make 1451+22 several times more massive than any supercluster yet investigated.

VI. FLAT VERSUS SPHERICAL SUPERCLUSTERS

There are two classes of theories to explain the existence of superclusters. In the isothermal models (Peebles and Dicke 1968; Peebles 1974; White and Rees 1978), primordial density perturbations in the early universe affected only the matter density, while the radiation density remained nearly homogeneous. The result of this scenario is hierarchical clustering, with globular cluster-sized objects condensing first as a result of Jeans instability and larger systems forming from gravitational interactions. Under these conditions, it is difficult to form flat or filamentary-shaped superclusters in a Hubble time.

An alternative scenario proposes that the fluctuations before decoupling were adiabatic in nature, affecting both the matter and radiation density (Sunyaev and Zel'dovich 1972; Zel'dovich 1978; Doroshkevich, Shandarin, and Saar 1978). In this picture, structures with scale lengths of superclusters formed first, since perturbations involving small masses are damped out in radiation-dominated plasma. Clusters of galaxies and individual galaxies were then formed from the fragmentation of these protocluster gas clouds. This scheme very nicely explains flat and/or filamentary-shaped superclusters, since the clouds could have collapsed to pancakes before galaxy formation began (Doroshkevich *et al.* 1980; Dekel 1983). The problems, however, occur in trying to create galaxies before $z \sim 3$ and in keeping the microwave background homogeneous to the degree observed.

The observations of 1451+22 seem to support the adiabatic theory of formation. Except for the central degree of the supercluster, the density profile appears flat with radius, with enhancements in one and possibly two filaments running through the center of the system. With this interpretation, the low velocity dispersion measured by CFBH translates into a supercluster thickness of only $\sim 15h^{-1}$ Mpc and implies a projected length-to-depth axis ratio for the system of $\sim 3:1$. This

makes the supercluster look very much like a Zel'dovich pancake.

However, the galaxy counts by themselves do not exclude spherical systems. Although the number of measured supercluster galaxies is large, it may not be large enough to avoid the effect of statistical fluctuations. In addition, if the supercluster galaxy density declines rapidly with radius, the recorded density profile may mimic that of an intrinsically flat system. To investigate these possibilities, a series of model spherical superclusters was created.

To best reproduce the observed supercluster, 1451+22 was modeled as a large collection of galaxy groups and clusters, with a distribution of luminosities satisfying the Gott and Turner (1977) multiplicity function. (When normalized to the total supercluster luminosity derived above, this relation predicts 10 Abell clusters for 1451+22—a number in good agreement with the seven observed.) Galaxies obeying the Schechter luminosity function were then divided randomly among these clusters, making sure that no group received more than its share of luminosity. Next, within each cluster, random positions for the galaxies were selected, under constraints imposed by spherical symmetry and a King (1972) radial distribution. Finally, these clusters were spherically distributed within the supercluster, using three different radial profiles: a uniform distribution, a $1/r$ radial distribution, and an inverse-square law radial distribution. In order to estimate the possible variations in the measured density profile, 50 models were run in each series.

Figures 8 and 11 compare the observed E/S0 number counts and the luminosity density enhancements with those calculated for the spherical models. The inverse-square law density profile is the only curve which is totally unacceptable, but none of the models work very well. Although the surface density profile of the uniform sphere does have the small slope needed to reproduce the data at large radii, the shape of the curve is wrong, and the model severely underestimates the number of galaxies at the center of the supercluster. This latter condition is improved in the model which uses a linear density gradient, but between 3° and 4° the surface density falls off too fast compared with the observations. The small range of values

found in the Monte Carlo simulations rule out invoking statistical fluctuations to explain the discrepancies in the models. Yet, given a proper variation of galaxy density with radius, it may still be possible to reproduce the observations with spherical systems.

If 1451+22 is a pancake, the density enhancement of galaxies is relatively high, with $\rho/\rho_{\text{field}} \approx 10$. This value is very much in line with that found for two other superclusters. By modeling the velocity field of the Local Supercluster, Yahil, Sandage, and Tammann (1980) derived a density contrast of 4 for this very poor system. In the richer Coma Supercluster, Oort (1983) found a density contrast of ~ 8.4 through the number density enhancement of Shapley-Ames galaxies with $6000 < v_{\text{rad}} < 8000 \text{ km s}^{-1}$. Since 1451+22 is the richest system studied to date, 10 is a very reasonable number for the density contrast. However, for the case of a flat supercluster, because the observed radial velocities reflect the primordial galaxy distribution, the redshifts cannot be used to probe the total matter density in the supercluster.

If the supercluster is actually a quasi-spherical system, the density contrast of the system is roughly $\rho/\rho_{\text{field}} \sim 6$. In this case, the small velocity dispersion must be due to gravitational slowing of the Hubble expansion, and the dynamical information leads to some interesting astrophysical quantities. Ford *et al.* (1981) modeled 1451+22 using noncrossing spherical mass shells, and obtained a total mass density for the supercluster of $\sim 1.5\rho_{\text{critical}}$. When applied to the luminosity density derived in § V, this implies that the mass-to-light ratio integrated over the entire supercluster is $(M/L)_{\odot} \sim 130h$. If the mass-to-light ratio is the same both inside and outside the supercluster, the density contrast calculated above becomes very important, since it yields a density parameter for the universe of $\Omega_0 \sim 0.3$.

VII. DISCUSSION

In the luminosity contour map of Figure 7, the most conspicuous feature is the stream of galaxies which extends southeast from Abell 1972 and goes through the clusters Abell 1980, 1986, and probably 1988. Both the structure and the galaxy content of this primary filament is reminiscent of that found for the chain of clusters defining the Pisces-Perseus supercluster. As in the case of Perseus (Gregory, Thompson, and Tifft 1981), redshift information suggests that the filament is thin not only in width but also in depth (CFBH). Also as in Perseus (Giovanelli, Haynes, and Chincarini 1986), the fraction of early-type galaxies in this filament is greater than that of its lower density surroundings, indicating that some degree of

morphological segregation has occurred. Unlike the situation for the Pisces-Perseus chain, however, a substantial amount of 1451+22's luminosity lies outside this region. Abell clusters 1976 and 2001 are aligned with Abell 1986 perpendicular to the primary filament, while most of the CFBH small groups are outside the central Abell cluster core and have no connection with either chain. As can be seen in Figure 7, the field of 1451+22 contains several large-scale linear structures. Since this supercluster is one of the richest known, 1451+22's morphology might be the result of the intersection of two Perseus-type systems. A single chain of clusters, however, cannot explain the observed distribution.

One of the difficulties in performing comparisons between a supercluster and the field is defining just what the "field" is. In modeling 1451+22 we assumed that the supercluster was a simple density enhancement on top of a uniform and homogeneous background. This is almost certainly not the case. Zel'dovich, Einasto, and Shandarin (1982) have proposed that the universe is mostly composed of voids, with all galaxies grouped into sheets and filaments which fill only $\sim 1\%$ of space. More recently, Gott, Melott, and Dickinson (1986) have characterized the universe as having spongelike topology, with equivalent and interconnecting high- and low-density regions. If either of these morphologies exists, then supercluster-field comparisons of the type made here are considerably more difficult. By measuring two control fields totaling ~ 40 square degrees and located far away from the supercluster on the sky, the hope was to average over local fluctuations in the galaxy background and obtain an accurate determination of the general field. However, it is quite possible that much larger regions are needed for this purpose. If the control fields contain a major void or supercluster near the redshift of 1451+22, then the results of the differential analysis performed here may have a large uncertainty.

I wish to thank Ed Kibblewhite and the APM group for their efforts in the plate digitization, and especially Mike Irwin for allowing me access to the APM reduction software. Thanks also go to Rex Rivolo and Dave Koo, who shared with me many useful insights on superclustering. I am indebted to Mike Potter and Mike Jewison, who digitized sample regions of my Schmidt plates with the Space Telescope's PDS machines, and to Mike Shara and Mike Potter for obtaining the photometric CCD observations in Israel. Extra special thanks go to Holland Ford for his continued interest, advice, and support (financial and otherwise) in this work.

REFERENCES

- Abell, G. O. 1958, *Ap. J. Suppl.*, **3**, 211.
 ———. 1982, private communication.
 Bahcall, J. N., and Soneira, R. M. 1980, *Ap. J. Suppl.*, **44**, 73.
 ———. 1981a, *Ap. J. Suppl.*, **47**, 357.
 ———. 1981b, *Ap. J.*, **246**, 122.
 Bhavsar, S. P., and Barrow, J. D. 1983, in *Clusters and Groups of Galaxies*, ed. F. Mardirossian, G. Giuricin, and M. Mezzetti (Dordrecht: Reidel), p. 415.
 Bunclark, P. S., and Irwin, M. J. 1984, in *IAU Colloquium 78, Astronomy with Schmidt-Type Telescopes*, ed. M. Capaccioli (Dordrecht: Reidel), p. 147.
 Burstein, D., and Heiles, C. 1982, *A.J.*, **87**, 1165.
 Burstein, D., and McDonald, L. H. 1975, *A.J.*, **80**, 17.
 Butcher, H., Oemler, A., Tapia, S., and Tarenghi, M. 1976, *Ap. J. (Letters)*, **209**, L11.
 Chincarini, G., Rood, H. J., and Thompson, L. A. 1981, *Ap. J. (Letter)*, **249**, L47.
 Ciardullo, R., Ford, H., Bartko, F., and Harms, R. 1983, *Ap. J.*, **273**, 24 (CFBH).
 Coleman, G. D., Wu, C. C., and Weedman, D. W. 1980, *Ap. J. Suppl.*, **43**, 3093.
 Couch, W. J., and Newell, E. B. 1984, *Ap. J. Suppl.*, **56**, 143.
 Davis, M., Geller, M. J., and Huchra, J. P. 1979, *Ap. J.*, **221**, 1.
 Dekel, A. 1983, *Ap. J.*, **264**, 373.
 de Vaucouleurs, G. 1975a, *Ap. J.*, **202**, 319.
 ———. 1975b, *Ap. J.*, **202**, 610.
 de Vaucouleurs, G., and de Vaucouleurs, A. 1972, *Mem. R.A.S.*, **77**, 1.
 de Vaucouleurs, G., de Vaucouleurs, A., and Corwin, H. G., Jr. 1976, *Second Reference Catalogue of Bright Galaxies* (Austin: University of Texas).
 Doroshkevich, A. G., Kotok, E. v., Novikov, I., Polyudov, A. N., Shandarin, S. F., and Sigov, Yu. S. 1980, *M.N.R.A.S.*, **192**, 321.
 Doroshkevich, A. G., Shandarin, S. F., and Saar, E. 1978, *M.N.R.A.S.*, **184**, 643.
 Doroshkevich, A. G., Sunyaev, Ra. A., and Zel'dovich, Ya. B. 1974, in *IAU Symposium 63, Confrontation of Cosmological Theories with Observational Data*, ed. M. S. Longair (Dordrecht: Reidel), p. 213.
 Ellis, R. S. 1982, in *The Origin and Evolution of Galaxies*, ed. B. J. T. Jones and J. E. Jones (Dordrecht: Reidel), p. 255.
 Faber, S. M., and Gallagher, J. S. 1979, *Ann. Rev. Astr. Ap.*, **17**, 135.
 Felten, J. E. 1977, *A.J.*, **82**, 861.
 Fontanelli, P. 1984, *Astr. Ap.*, **138**, 85.
 Ford, H. C., Harms, R. J., Ciardullo, R., and Bartko, F. 1981, *Ap. J. (Letters)*, **245**, L53.
 Giovanelli, R., Haynes, M. P., and Chincarini, G. L. 1986, *Ap. J.*, **300**, 77.

- Gott, J. R., Melott, A. L., and Dickinson, M. 1986, *Ap. J.*, **306**, 341.
 Gott, J. R., and Turner, E. L. 1977, *Ap. J.*, **216**, 357.
 Gregory, S. A., and Thompson, L. A. 1978, *Ap. J.*, **222**, 784.
 Gregory, S. A., Thompson, L. A., and Tift, W. G. 1981, *Ap. J.*, **243**, 411.
 Hammersley, J. M., and Welsh, D. J. A. 1980, *Contemp. Phys.*, **21**, 593.
 Hoessel, J. G., Gunn, J. E., and Thuan, T. X. 1980, *Ap. J.*, **241**, 486.
 Huchra, J. P. 1978, in *IAU Symposium 79, The Large Scale Structure of the Universe*, ed. M. S. Longair and J. Einasto (Dordrecht: Reidel), p. 271.
 Jarvis, J. F., and Tyson, J. A. 1981, *A.J.*, **86**, 476.
 Kibblewhite, E. J. 1980, *APM Facility Manual* (Cambridge: Institute of Astronomy).
 King, I. R. 1972, *Ap. J. (Letters)*, **174**, L123.
 King, C. R., and Ellis, R. 1985, *Ap. J.*, **288**, 456.
 Kirschner, R. P., Oemler, A., and Schechter, P. L. 1979, *A.J.*, **84**, 951.
 Kirschner, R. P., Oemler, A., Schechter, P. L., and Shectman, S. A. 1981, *Ap. J. (Letters)*, **248**, L57.
 Koo, D. 1986, private communication.
 Kron, R. G. 1980, *Ap. J. Suppl.*, **43**, 305.
 Kuhn, J. R., and Uson, J. M. 1982, *Ap. J. (Letters)*, **263**, L47.
 Landolt, A. U. 1983, *A.J.*, **88**, 439.
 Lasker, B. 1985, private communication.
 Low, F. J., et al. 1984, *Ap. J. (Letters)*, **278**, L19.
 Lucey, J. R., Dickens, R. J., Mitchell, R. J., and Dawe, J. A. 1983, *M.N.R.A.S.*, **203**, 545.
 Moody, J. E., Turner, E. L., and Gott, J. R., III. 1983, *Ap. J.*, **273**, 16.
 Oort, J. H. 1983, *Ann. Rev. Astr. Ap.*, **21**, 373.
 Peebles, P. J. E. 1974, *Ap. J. (Letters)*, **189**, L51.
 Peebles, P. J. E., and Dicke, R. H. 1968, *Ap. J.*, **154**, 891.
 Pence, W. 1976, *Ap. J.*, **203**, 39.
 Peterson, B. A., Ellis, R. S., Kibblewhite, E. J., Bridgeland, M., Hooley, T., and Horne, D. 1979, *Ap. J. (Letters)*, **233**, L109.
 Peterson, B. M. 1978, *Ap. J.*, **223**, 740.
 Sandage, A. 1973, *Ap. J.*, **183**, 711.
 Schechter P. L. 1976, *Ap. J.*, **203**, 297.
 Schneider, D. P., Gunn, J. E., and Hoessel, J. G. 1983, *Ap. J.*, **264**, 337.
 Shanks, T., Stevenson, P. R. F., Fong, R., and MacGillivray, H. T. 1984, *M.N.R.A.S.*, **206**, 767.
 Strom, K. M., and Strom, S. E. 1978, *A.J.*, **83**, 73.
 Sturch, C., et al. 1984, *Bull. AAS*, **16**, 498.
 Sunyaev, R. A., and Zel'dovich, Ya. B. 1972, *Astr. Ap.*, **20**, 189.
 Tammann, G. A., Yahil, A., and Sandage, A. 1979, *Ap. J.*, **234**, 775.
 Tarengi, M., Chincarini, G., Rood, H. J., and Thompson, L. A. 1980, *Ap. J.*, **235**, 724.
 Tarengi, M., Tift, W. G., Chincarini, G., Rood, H. J., and Thompson, L. A. 1979, *Ap. J.*, **234**, 793.
 Trumpler, R. J., and Weaver, H. F. 1953, in *Statistical Astronomy* (Berkeley: University of California Press), p. 127.
 Tully, R. B. 1982, *Ap. J.*, **257**, 389.
 Ulrich, M.-H. 1978, *Ap. J.*, **221**, 422.
 White, S. D. M., and Rees, M. J. 1978, *M.N.R.A.S.*, **183**, 341.
 Yahil, A., Sandage, A., and Tammann, G. A. 1980, *Ap. J.*, **242**, 448.
 Zel'dovich, Ya. B. 1978, in *IAU Symposium 79, The Large Scale Structure of the Universe*, ed. M. S. Longair and J. Einasto (Dordrecht: Reidel), p. 409.
 Zel'dovich, Ya. B., Einasto, J., and Shandarin, S. F. 1982, *Nature*, **300**, 407.

ROBIN CIARDULLO: Department of Terrestrial Magnetism, Carnegie Institute of Washington, 5241 Broad Branch Road, N.W., Washington, DC 20015